

Article

Assessing Recharge Sources and Seawater Intrusion in Coastal Groundwater: A Hydrogeological and Multi-Isotopic Approach

Maria Chiara Porru¹, Claudio Arras¹, Riccardo Biddau¹, Rosa Cidu¹, Francesca Lobina¹, Francesca Podda¹, Richard Wanty² and Stefania Da Pelo^{1,*}

- ¹ Department of Chemical and Geological Sciences, University of Cagliari, Campus of Monserrato, 09042 Monserrato, Italy; mariac.porru@unica.it (M.C.P.); claudio.arras@unica.it (C.A.); riccardo.biddau@unica.it (R.B.); cidur@unica.it (R.C.); francesca.lobina@unica.it (F.L.); fpodda@unica.it (F.P.)
- ² Department of Geology and Geological Engineering, Colorado School of Mines, Golden, CO 80401, USA; rwanty@mines.edu
- * Correspondence: sdapelo@unica.it

Abstract: One of the crucial challenges of our time is climate change. The consequences of rising sea levels and drought greatly impact water resources, potentially worsening seawater intrusion. Characterizing coastal aquifers is an essential step in devising strategies to address these phenomena. Seawater intrusion poses a critical socio-economic and environmental issue in the coastal plain of Muravera, southeastern Sardinia (Italy). This coastal plain is an important agricultural area in Sardinia, and the health of the crops is compromised by the increasing salinization of shallow groundwater. To enhance our understanding of the hydrogeological conceptual model, which is essential for a sustainable resource management system, hydrogeological investigations were conducted and complemented by the chemical and multi-isotopic analyses of groundwater. The main objectives of this study were to identify groundwater recharge areas, understand salinization mechanisms and trace the evolution of water chemistry. Within this framework, a monthly survey monitoring piezometric level and electrical conductivity was carried out for one year. This survey was integrated with chemical and isotope analyses, including $\delta^{18}\text{O}_{\text{H}_2\text{O}}$ and $\delta^2\text{H}_{\text{H}_2\text{O}}$, $\delta^{11}\text{B}$, $\delta^{18}\text{O}_{\text{SO}_4}$, $\delta^{34}\text{S}_{\text{SO}_4}$, and $^{87}\text{Sr}/^{86}\text{Sr}$. Hydrochemistry analysis results revealed the occurrence of seawater–freshwater mixing, extending up to 4 km inland. H_2O isotope analysis confirmed the mixing processes and indicated the meteoric origin of recharge waters for both shallow and semi-confined aquifers. The strontium isotopes ratio facilitated the identification of four main groundwater flow paths, confirmed by the SIAR model. The results of this combined hydrogeological–geochemical–isotopic survey provide essential elements for the future implementation of an integrated and sustainable management system. These findings enable interventions to slow the process of seawater intrusion and meet the economic needs for the development of local communities.

Keywords: coastal aquifers; salinization; hydrochemistry; isotopes; Muravera plain; Sardinia; SIAR



Citation: Porru, M.C.; Arras, C.; Biddau, R.; Cidu, R.; Lobina, F.; Podda, F.; Wanty, R.; Da Pelo, S. Assessing Recharge Sources and Seawater Intrusion in Coastal Groundwater: A Hydrogeological and Multi-Isotopic Approach. *Water* **2024**, *16*, 1106. <https://doi.org/10.3390/w16081106>

Academic Editor: Micòl Mastrocicco

Received: 14 March 2024

Revised: 2 April 2024

Accepted: 9 April 2024

Published: 12 April 2024



Copyright: © 2024 by the authors. Licensee MDPI, Basel, Switzerland. This article is an open access article distributed under the terms and conditions of the Creative Commons Attribution (CC BY) license (<https://creativecommons.org/licenses/by/4.0/>).

1. Introduction

Seawater intrusion (SI) is a global phenomenon that occurs in many coastal aquifers and is increasing dramatically. Researchers worldwide have extensively discussed this phenomenon due to its significant impact on water resource depletion [1–4]. The combination of rising sea levels resulting from climate change, coupled with severe over-exploitation and the mismanagement of water, exacerbates these effects. In the Mediterranean area, a continuous increase in the salinization of coastal regions, in terms of both the number and size of affected areas, has been observed to varying extents [5]. In Sardinia (Italy), climate projections indicate that the region will experience a general increase in temperatures, both in average and extreme values, as well as a reduction in annual precipitation. Additionally, there will be a higher intensity and frequency of extreme weather events, including

Due to the geological complexity of the plain and the intrusion of seawater, numerous hydrogeological, geological, and geophysical studies have been carried out since 1970 [18–27]. Despite the large number of investigations, many aspects remain unclear.

Through a multidisciplinary approach, this work aims to provide a methodology to (1) offer information about flow pathways, surface- and groundwater interactions, and all other possible recharge sources, including potential recharge from a sewage treatment plant's discharge to the alluvial aquifer through the surface channel where it is discharged; and (2) trace the evolution of water chemistry and salinization mechanisms, focusing on groundwater residence time.

The applied approach involved monthly monitoring campaigns to define piezometric trends and identify variations in chemical and physical parameters throughout an entire year. Additionally, water sampling for chemical and multi-isotopic analysis was performed. This methodology allows us to recognize recharge sources, flow pathways, surface- and groundwater interactions, and residence times. All these details are important for a comprehensive understanding of the system under study, helping to define salinization processes [13,28], contributing to designing intervention measures, and developing an integrated and sustainable groundwater management system.

2. Materials and Methods

2.1. Study Area

The Muravera Plain is located on the southeastern coast of Sardinia (Italy) and spans an area of 39 square kilometers. Annual rainfall in the plain varies between 200 and 1100 mm, with a prolonged drought period and an average annual temperature of approximately 18 °C. Within the plain, there are over 400 hectares of citrus groves and 227 hectares of rice fields, which represent a culturally significant aspect of the socio-economic development of the area. Moreover, during summertime, when water demand rises due to irrigation and tourism, uncontrolled groundwater exploitation occurs. An estimate of withdrawals indicates that more than 4 Mm³ of groundwater are extracted annually, against an estimated zenithal recharge varying from approximately 2 to about 4 Mm³ per year [29,30], emphasizing the necessity to establish a water balance. Despite being crossed by the Flumendosa River (the second longest river in Sardinia, 122 km), the plain faces challenges due to several dams along its watershed, leading to a reduction in runoff water to the plain and an as-yet unquantified recharge to the groundwater. Several torrential tributaries, including the Flumini Uri, Rio Pibilia, Riu Mannu, and Riu de Su Fenugraxiu, flow into the Flumendosa within the plain area. Furthermore, the inland area behind the coastline is characterized by the presence of the abandoned arms of the river (known as Foxi) and the Sa Praia Pond (Figure 1), both of which have become salinized due to a direct opening to the sea for aquaculture activities.

From a geological point of view, the plain area is mostly represented by Holocene alluvial deposits related to the ancient-to-actual activity of the Flumendosa River; Pleistocene continental deposits widely outcrop along the southern border of the plain and within the main tributaries' valleys (i.e., Riu Pibilia, Flumini Uri and Riu Su Fenugraxiu). The plain is surrounded by hilly reliefs where low-grade metamorphic rocks of the Sardinian Paleozoic basement mainly outcrop.

A high-productivity porous aquifer is hosted within the Holocene alluvium, which reaches a maximum thickness of 50 m; the aquifer is mostly phreatic in the western part of the plain, while moving eastward, the occurrence of silt and clay deposit intercalations, with variable extension and thickness, produce the local confinement of the aquifer [30]. Low-productivity aquifers are hosted within the Pleistocene alluvial deposits (gravel and sand cemented) and the metamorphic basement and can contribute to the lateral recharge of the alluvial aquifer.

2.2. Hydrogeological Surveys and Geochemical Campaigns

The hydrogeological monitoring activities were carried out between June 2020 and May 2021 to encompass an entire year and observe possible seasonal variations. These activities involved the monthly measurement of piezometric heads and the main physical-chemical parameters, namely electrical conductivity (EC), pH, and temperature, at approximately 80 points, including both surface- and groundwaters (Figure 2a). As some of these points included private wells, which were not always accessible, during certain campaigns, specific points were either not monitored or replaced by nearby points with similar characteristics. Two geochemical campaigns were conducted, one at the turn of September and October 2020 and one in June 2022. Sampling was typically performed in the dynamic parameter-stabilized mode following the low-flow methodology [31]. At selected sites, both static and dynamic sampling were conducted. Water samples were filtered in situ through polycarbonate filters with an all-plastic filtration assembly (Sartorius Stedim Biotech GmbH, Gottinger, Germany) at 0.22 μm for major ions and isotopes and at 0.45 μm for metals. After filtration, samples for metal analyses were acidified with 1% HNO_3 (68% Suprapur, Carlo Erba reagents srl Cornaredo (MI), Cornaredo, Italy), while those for $\delta^{34}\text{S}_{\text{SO}_4}$ $\delta^{18}\text{O}_{\text{SO}_4}$ were acidified with HCl (35% Suprapur Carlo Erba, 2 mL in 1 L of sample). At each sampling site, measurements were taken for temperature (Checktemp Dip, Hanna instruments©, Woonsocket, RI, USA), pH (Thermo scientific™ Orion™, Ross pH electrode, Waltham, MA, USA), Eh (oxidation-reduction potential, Thermo scientific™ Orion™), alkalinity (AF microdosimeter, AFGTC, San Giuliano Terme (PI), Italy), dissolved oxygen (Oxygen Kit, Carlo Erba Idrimeter), and conductivity (Cond 315i WTW GmbH, Weilheim, Germany). The Eh was measured using a platinum electrode, and the value was corrected against Zobell's solution [32]. Alkalinity was determined by acidimetric titration using methyl orange (as an indicator, Merck KGaA, Darmstadt, Germany) and expressed as bicarbonate ion (HCO_3^-), as CO_3^{2-} was consistently undetectable, and the contribution of non-carbonate species was negligible.

Based on the geometry of the Muravera aquifer [30], the possible sources of recharging (like rivers and lateral aquifer), and results from the hydrogeological monitoring, a total of 53 water points were selected for geochemical and isotope investigations in 2020, comprising the following:

- A total of 44 groundwater samples were collected from various aquifers: 30 from the alluvial phreatic aquifer, 10 from the alluvial semiconfined aquifer, 1 from the metamorphic basement, and 4 from the Pleistocene alluvial aquifer. The latter were selected to identify potential sources of lateral recharge to the plain.
- A total of 9 surface water samples, including 7 from the Flumendosa River and the Foxi, 1 from the mouth of the S. Giovanni fishpond (where lagoon waters mix with seawater, named SW*), and 1 from the discharge of the urban sewage treatment plant (sample 1). The latter was collected to assess possible recharge to the alluvial aquifer.

A total of 15 points were sampled in 2022, 13 of which had already been sampled in both 2020 and 2022, with 6 of these being sampled both statically and dynamically (points 7, 8, 9, 26, 36, and 44), resulting in a total of 74 samples.

All the samples underwent analysis for chemicals and $\delta^{18}\text{OH}_2\text{O}$ and $\delta^2\text{HH}_2\text{O}$ analyses (Figure 2b).

Additionally, $\delta^{11}\text{B}$, $\delta^{18}\text{OSO}_4$ and $\delta^{34}\text{SSO}_4$, and $^{87}\text{Sr}/^{86}\text{Sr}$ were analyzed at 38 selected water sampling points (Figure 2):

- In total, 30 groundwater samples were collected from the Holocene alluvial phreatic and semi-confined aquifers (25 samples), Pleistocene alluvial aquifer (4 samples), and metamorphic basement (1 sample).
- In total, 8 surface water samples were collected from the Flumendosa River (6 samples), the discharge of the sewage treatment plant (1 sample), and the SW* (1 sample).

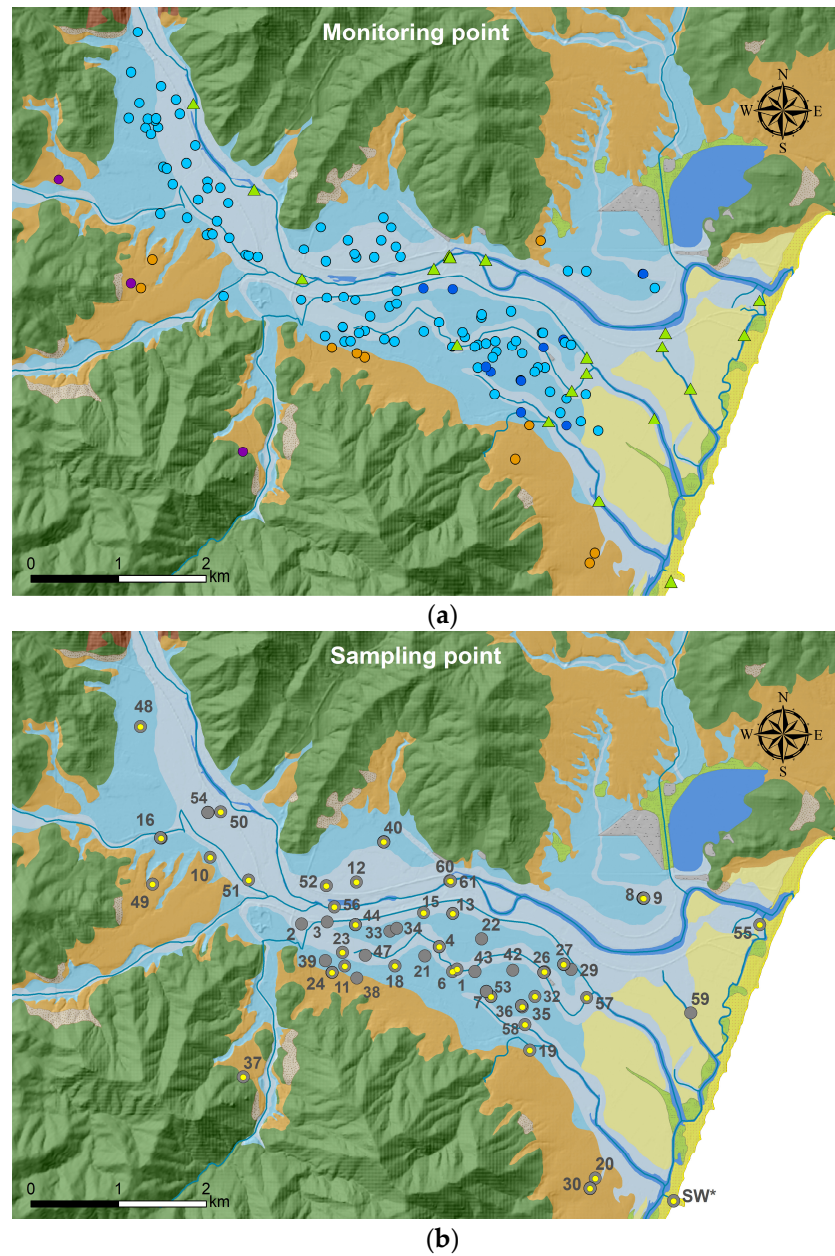


Figure 2. Location of points monitored for one year of monthly hydrogeological surveys (a) and points sampled during the two campaigns for geochemical and isotope characterization (b).

Details on analytical methods and laboratories are shown in Table 1. For $\delta^{34}\text{S}_{\text{SO}_4}$ and $\delta^{18}\text{O}_{\text{SO}_4}$ analyses, dissolved SO_4^{2-} was precipitated as BaSO_4 by adding $\text{BaCl}_2 \cdot 2\text{H}_2\text{O}$ after acidifying the sample with HCl and boiling it to prevent BaCO_3 precipitation, following standard methods [33].

Table 1. Methodologies used for the analyses. ICP-OES (Optical Emission Spectrometry); IC (Ionic Chromatography), ICP-MS (Mass Spectrometry), MC-ICP-MS (Multiple Collector Inductively Coupled Plasma Mass Spectrometry), EA-IRMS (Elemental Analyzer Isotope Ratio Mass Spectrometry) and High Temperature Conversion EA-IRMS (TC-EA-IRMS).

Analyte	Analytical Methods	Laboratory
Major ions	ICP-OES (Agilent 5110, Santa Clara, CA, USA) IC (Thermo Fisher, Dionex ICS3000)	University of Cagliari, (Italy)
Trace elements	ICP-OES and ICP-MS (PerkinElmer SCIEX ELAN DRC-e, Milan, Italy),	University of Cagliari, (Italy)
$\delta^2\text{H}_{\text{H}_2\text{O}}$ $\delta^{18}\text{O}_{\text{H}_2\text{O}}$	Off-Axis Integrated Cavity Output Spectroscopy (OA-ICOS), LWIA-45-EP, Los Gatos, Mountain View, CA)	University of Cagliari, (Italy)
$^{87}\text{Sr}/^{86}\text{Sr}$	MC-ICP-MS (Thermo Neptune Plus)	CNR-IGG, Pisa, (Italy)
$\delta^{11}\text{B}$	MC-ICP-MS MS (Thermo Neptune Plus)	CNR-IGG, Pisa, (Italy)
$\delta^{34}\text{S}_{\text{SO}_4}$ $\delta^{18}\text{O}_{\text{SO}_4}$	EA-IRMS and TC-EA-IRMS (Carlo Erba 1108 coupled with a Thermo Delta C Finnigan Mat)	University of Barcelona, (Spain)

To ensure high analytical quality, nearly all chemical elements, including major ions and those crucial for defining seawater intrusion processes, such as boron, strontium, and bromine, were determined using multiple techniques. The analytical goodness of the performed analyses was assessed through the ionic balance, precision, and accuracy. The ionic balance consistently fell within the range of $\pm 5\%$; both precision and accuracy were estimated at 15% or better, using randomly duplicate samples and a standard reference solution (EnviroMAT™ EP-L-3, Baie D'Urfé, Quebec, QC, Canada). For the strontium isotope, values were adjusted based on the measured mean value for the SRM NIST 987 standard (Gaithersburg, MD, USA) with reference to the $^{87}\text{Sr}/^{86}\text{Sr}$ value of 0.710248 [34]. The effect of instrumental fractionation on the $^{11}\text{B}/^{10}\text{B}$ ratio of the samples was corrected using the bracketing method (sequence: blank-standard-blank-sample-blank-standard-blank). Analytical errors, calculated from randomly duplicate samples or using international and internal laboratory standards, were as follows: 0.1‰ for $\delta^2\text{H}$, 0.05‰ for $\delta^{18}\text{O}_{\text{H}_2\text{O}}$, $2 \times 10^{-5}\%$ for $^{87}\text{Sr}/^{86}\text{Sr}$; 0.05‰ for $\delta^{11}\text{B}$, 0.2‰ for $\delta^{34}\text{S}_{\text{SO}_4}$, and 0.5‰ for $\delta^{18}\text{O}_{\text{SO}_4}$. Isotopic results were expressed in terms of δ [35] relative to the international standard Vienna Standard Mean Oceanic Water (V-SMOW) for $\delta^2\text{H}$, $\delta^{18}\text{O}_{\text{H}_2\text{O}}$, $\delta^{18}\text{O}_{\text{SO}_4}$; the Vienna Canyon Diablo Troilite (V-CDT) for $\delta^{34}\text{S}$; and NBS951 for $\delta^{11}\text{B}$.

3. Results and Discussion

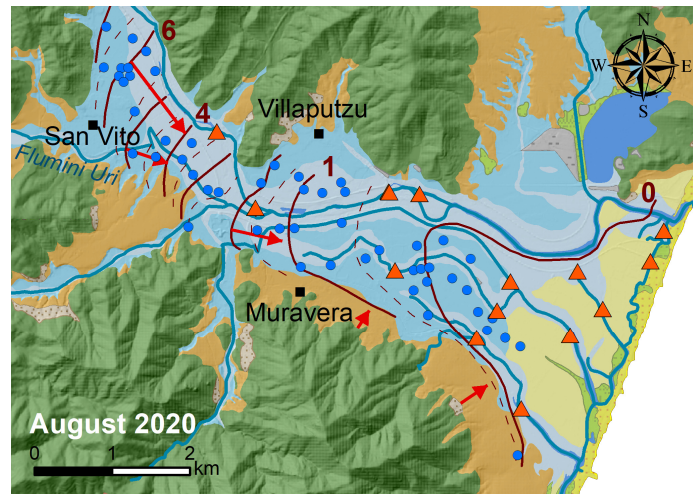
3.1. Hydrogeological Survey

In the alluvial aquifer, piezometric heads gently decreased from approximately 8 m asl in the north-western part of the plain towards the sea with a medium gradient of 1‰. In the Pleistocene alluvial aquifer, the hydraulic gradient is much steeper (13‰) and reached values of 18 m asl (Figure 3).

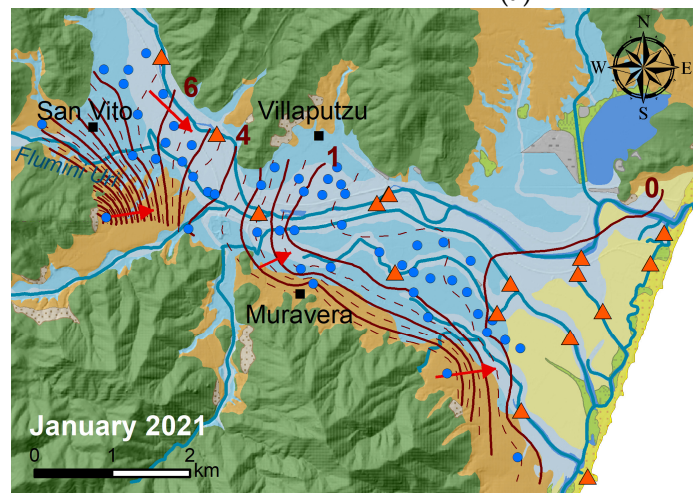
Interactions between the Flumendosa River and groundwater vary along the plain. Figure 3 shows that in the north-western part, the Flumendosa River is drained by the aquifer, while in the central part of the plain, downstream of Villaputzu village, the trend is reversed, and the aquifer is drained by the Flumendosa River. Recharge from the Flumini Uri River to the aquifer is also observed. The water table's zero level is approximately 2 km from the inland shoreline during the winter. In the summer, the piezometric head decreases by about 1.5 m across the entire plain, and the zero level moves inland by about 1 km.

In groundwater, the EC varies from a value of 0.2 mS/cm approximately 8 km inland, near Flumini Uri River (refer to Figure 4), to a maximum value of 23 mS/cm close to the coastline. Along the Flumendosa River, EC in the surface water increases from about 0.6 mS/cm upstream, close to the San Vito village, to 17 mS/cm downstream at the river mouth. Near the coast, the conductivity of surface water significantly increases, distinguishing itself from groundwater. Surface waters exhibit much higher EC values compared

to groundwater, ranging from 54 mS/cm at the fishpond (SW*) to about 30 mS/cm in the Foxi channels and Sa Praia Pond. Small seasonal variations in EC values were observed for both surface- and groundwater (Figure 4).



(a)



(b)

Legend

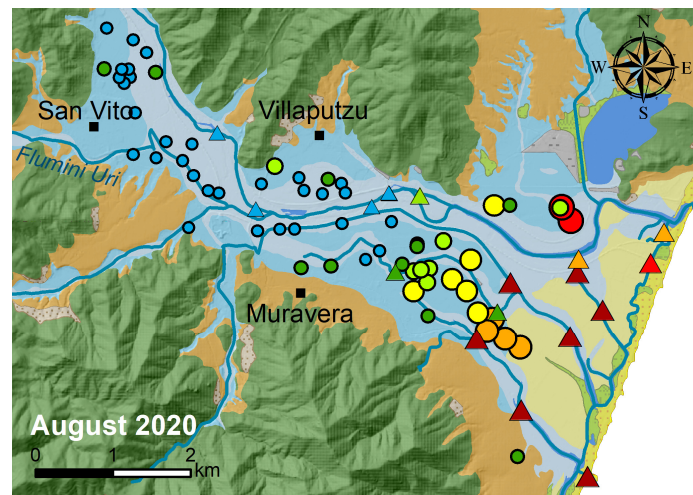
Geological setting

- h-Anthropogenic deposits
- a- Holocene slope deposits
- g2- Holocene beach deposits (sand and gravel)
- e- Holocene lake deposits (silt and clay)
- b- Holocene alluvial deposits (gravel, sand, silt, clay)
- g- Holocene ancient beach deposits (sand and clay)
- bna- Holocene terraced alluvial deposits (gravel and sand)
- PVM- Pleistocenic alluvial deposits (gravel and sand cemented)
- MET- Paleozoic metamorphic basement, metamorphosed sandstones
- IR- Paleozoic intrusive rocks, granitoids

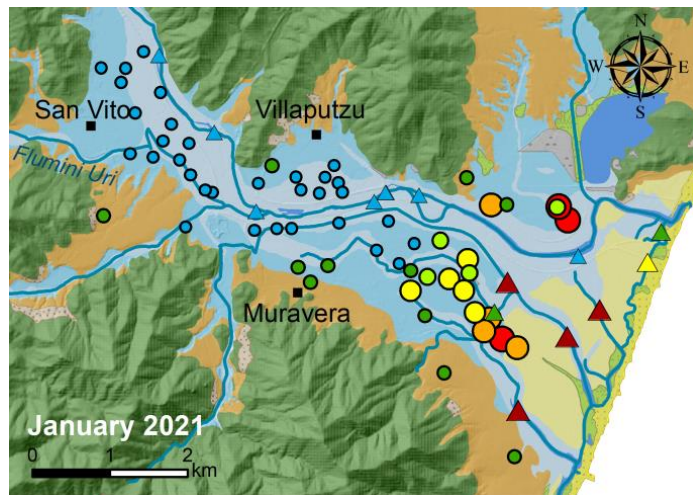
Other elements

- Water bodies
- Water level contour lines 1 m
- Water level contour lines 0.5 m
- Groundwater flow direction
- Groundwater
- Surface water

Figure 3. Comparison of piezometric contour lines in the summer ((a), August 2020) and winter ((b), January 2021). The numbers in the figure represent the piezometric level in m a.s.l.



(a)



(b)

Legend

Geological setting

- h-Anthropogenic deposits
- a- Holocene slope deposits
- g2- Holocene beach deposits (sand and gravel)
- e- Holocene lake deposits (silt and clay)
- b- Holocene alluvial deposits (gravel, sand, silt, clay)
- g- Holocene ancient beach deposits (sand and clay)
- bna- Holocene terraced alluvial deposits (gravel and sand)
- PVM- Pleistocene alluvial deposits (gravel and sand cemented)
- MET- Paleozoic metamorphic basement, metamorphosed sandstones
- IR- Paleozoic intrusive rocks, granitoids

Other elements

- Water bodies
- Δ Surface water
- \circ Groundwater

EC mS/cm

- <0.7
- 0.7–1.5
- 1.5–2.5
- 2.5–5.0
- 5.0–10.0
- 10.0–30.0
- >30.0

Figure 4. Comparison between EC values measured at monitoring points in August 2020 (a) and January 2021 (b).

3.2. Water Chemistry

All the samples were classified according to the Piper diagram presented in Figure 5.

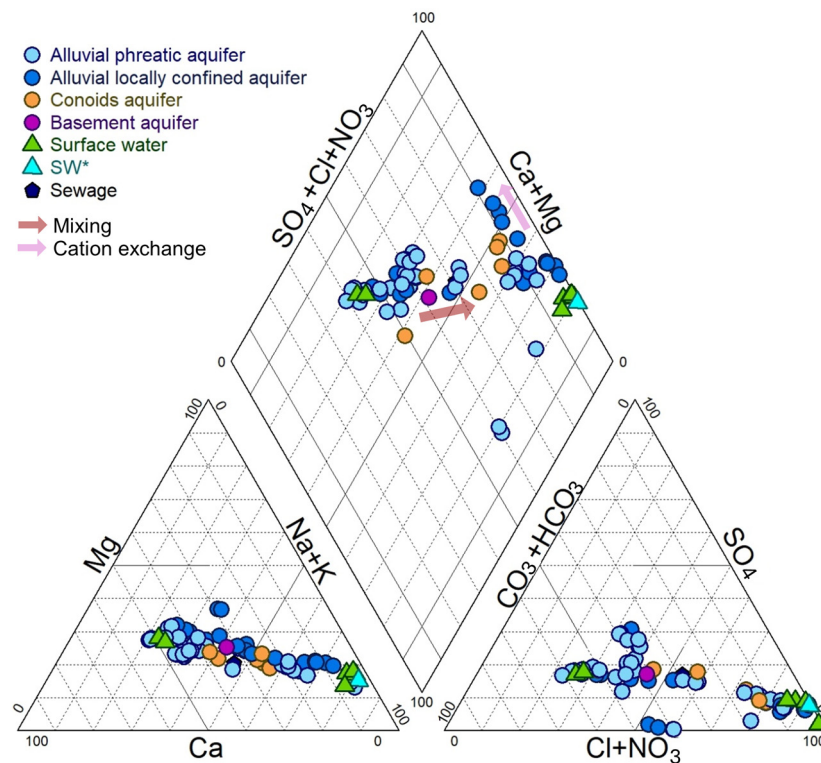


Figure 5. Piper diagram for the collected water samples in September/October 2020 and June 2022. (SW* S. Giovanni fishpond where lagoon waters mix with seawater).

The water chemistry of the Muravera Plain is regulated by different processes distinctive of saline intrusion (e.g., cation exchange, mixing). The more saline waters exhibited a sodium-chloride to calcium-chloride composition, while the less saline waters showed a bicarbonate-calcium to bicarbonate-calcium chloride character, with a weak sulfate contribution. Based on the chemical composition and the EC values of the samples, three groups of water were identified:

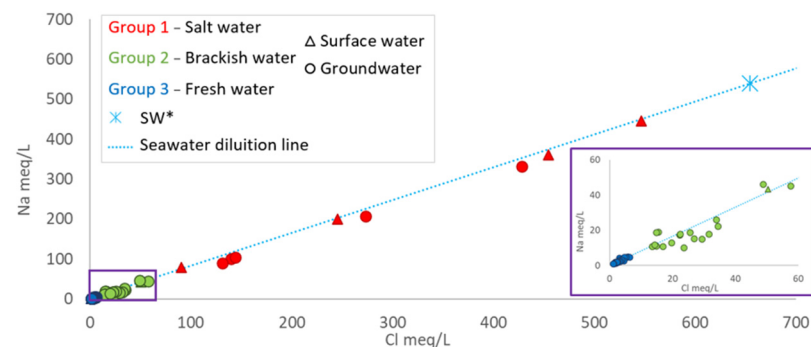
1. Group 1: Very salty waters: waters with Na-Cl composition and EC values higher than 10 mS/cm, indicating significant salinization processes.
2. Group 2: Brackish waters: groundwater samples with a Na-Cl composition and EC ranging from 2 to 10 mS/cm. These samples were collected approximately 2 to 4 km from the coast.
3. Group 3: Freshwater: waters with an HCO_3 -Ca composition and EC values lower than 0.8 mS/cm.

The summary statistics of selected elements for samples considered in this study are reported in Table 2 and in Table S1. The groundwater pH generally tended to be neutral, ranging from slightly acidic in freshwater to slightly alkaline in saline and brackish waters. Surface waters typically exhibited a higher alkaline pH, except when influenced by fresh groundwater, which can result in a slight acidity (i.e., sample 56). The redox potential and dissolved oxygen levels in surface waters indicated oxidation to transitional conditions, reflecting an oxygenated environment. Conversely, groundwater often exhibits more reducing conditions, especially in deep wells. Regarding chemical components, most of the samples exhibited a Na-Cl ratio that closely resembled that of seawater (Figure 6). However, the brackish waters (Group 2) deviated from this trend, appearing more dispersed around the seawater dilution line, implying a secondary process in addition to simple binary mixing.

Table 2. Summary statistics for samples collected in the Muravera plain.

	Groundwater					Surface Water			
	u.m.	Mean	Dv.St.	Min	Max	Mean	Dv.St.	Min	Max
T	°C	19	1.3	17	24	22	1.1	20	24
pH		7.0	0.4	6.4	8.1	7.6	0.50	6.9	8.2
EC	mS/cm	3	4.9	0.20	26	22	22	0.50	55
Eh	V	0.28	0.14	−0.14	0.58	0.28	0.10	0.25	0.32
O ₂	mg/L	4	1.9	0.70	9	8	2.9	3	13
Ca	mg/L	107	118	12	675	189	137	54	415
Mg	mg/L	84	173	6	1090	540	524	18	1240
Na	mg/L	471	1186	22	7630	4800	4854	29	12,400
K	mg/L	12	21	1.3	103	154	165	3	483
Cl	mg/L	962	2401	37	15,200	9060	9189	53	23,200
HCO ₃ [−]	mg/L	205	114	37	688	191	27	163	217
SO ₄ [−]	mg/L	138	253	3	1670	899	970	48	2640
NO ₃ [−]	mg/L	6	8.8	0.10	52	7	12	<1	32
NH ₄ ⁺	mg/L	7	7.2	0.20	22	<0.1	-	<0.1	<0.1
PO ₄	mg/L	4	6.0	0.10	16	0.1	-	<0.1	3
SiO ₂	mg/L	15	6.0	5	37	6	3.6	<1.4	12
Br	mg/L	3	7.5	0.09	47	30	36	0.20	91
B	µg/L	173	305	24	1510	1980	2197	32	5520
Sr	µg/L	572	978	77	5440	1180	1196	143	3120
Rb	µg/L	2.6	3.8	<0.01	17	55	52	<0.01	136

Seawater intrusion into the aquifer can result in Na depletion due to cation exchange [36,37] while freshening and/or calcite dissolution can control Ca enrichment. Carbonate dissolution may occur in a mixing zone despite both the freshwater and seawater end members being saturated with carbonates [38]. All the waters considered in this study were found to be undersaturated with respect to gypsum. Almost all of the Group 1 samples were undersaturated in calcite, while Group 2 samples were undersaturated in samples collected from the Pleistocene alluvial aquifer and shallow wells but were at equilibrium or oversaturated in deep wells. Group 3 was consistently oversaturated with respect to calcite.

**Figure 6.** Na vs. Cl. The seawater dilution line is derived from the chemical composition of local Sardinian seawater [39]. (SW*, S. Giovanni fishpond, where lagoon waters mix with seawater).

The same processes are evident in the Ca vs. Na graph (Figure 7a), where different trends are recognized. The first trend is observed in surface water, where increasing salinity (Group 1, in red in Figure 7) leads to an increase in the Na/Ca ratio compared to the seawater dilution line. Both the Foxi surface water (Group 1) and SW* sample follow this trend, indicating a simple mixing process. On the other hand, the groundwater of Group 1 follows a different trend, with a lower Na/Ca compared to seawater. This behavior may be attributed to the Ca-Na cation exchange processes, resulting from water interactions with the clayey matrix of the aquifer and facilitated by long interaction times. The SiO₂

vs. Sr graph in Figure 8, in fact, shows that groundwater samples in Group 1 have higher concentrations of both strontium and silica than seawater, which can be explained by prolonged water–rock interaction times. The groundwater for Group 2 and Group 3 had relatively consistent sodium concentrations, while calcium concentrations increased more rapidly. In freshwater samples (Group 3), the equivalent Ca-HCO₃ ratio was very close to one, suggesting that calcite may be the source of Ca in these waters. However, for saline and brackish waters, HCO₃ concentrations appeared to be controlled, highlighting the occurrence of exchange processes (Figure 7b).

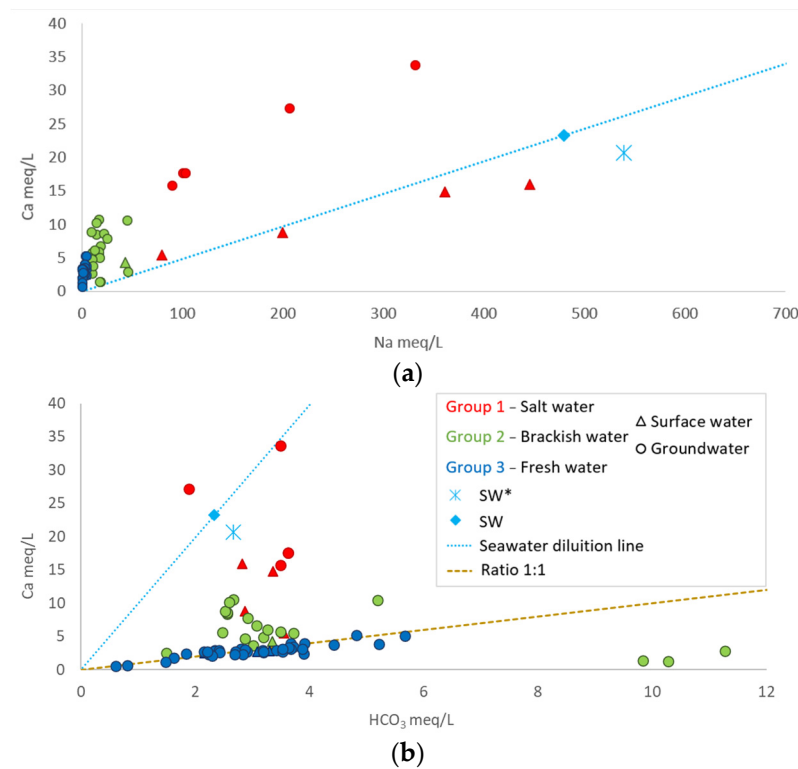


Figure 7. (a): Ca vs. Na; (b): Ca vs. HCO₃ (SW: Sardinian local seawater from [39]; SW*, S. Giovanni fishpond where lagoon waters mix with seawater).

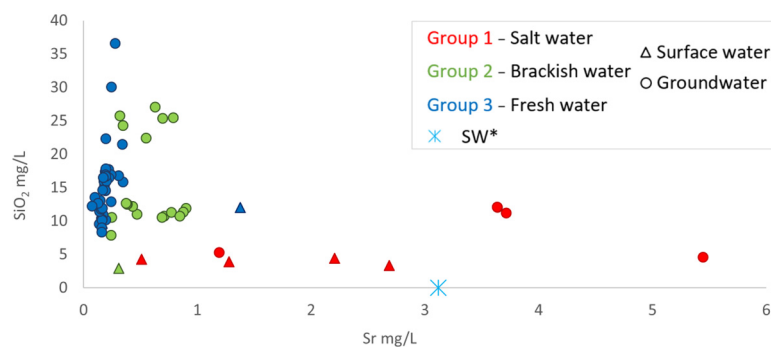


Figure 8. SiO₂ vs. Sr (SW*, S. Giovanni fishpond where lagoon waters mix with seawater).

3.3. Isotopic Composition

Stables isotopes in the groundwater system (Table 3) vary between -7.3 and 1.4‰ for $\delta^{18}\text{O}$ and between -42.3 and -8‰ for $\delta^2\text{H}$. Surface waters show values ranging from -5.5 e 0.15 and -30 $\delta^{18}\text{O}$ and 1.0 for $\delta^2\text{H}$. The SW* sample presents a $\delta^{18}\text{O} = 0.9\text{‰}$ and $\delta^2\text{H} = 6.5\text{‰}$, reflecting a slight evaporation from the local seawater signature ($\delta^{18}\text{O} = 0.6$ and $\delta^2\text{H} 4\text{‰}$, [40]), which is in agreement with other Mediterranean lagoon values [37,41]. According to the $\delta^{18}\text{O}$ — $\delta^2\text{H}$ isotopes data shown in Figure 9, most of the samples follow the

SIMWL (Southern Italy Meteoric Water Line [42]) and the GMWL (Global Meteoric Water Line [43]), proving the meteoric origin of the recharging water. Some samples in Group 1 have isotopic values that can be correlated with a mixing process between freshwater and lagoon water (namely SW*).

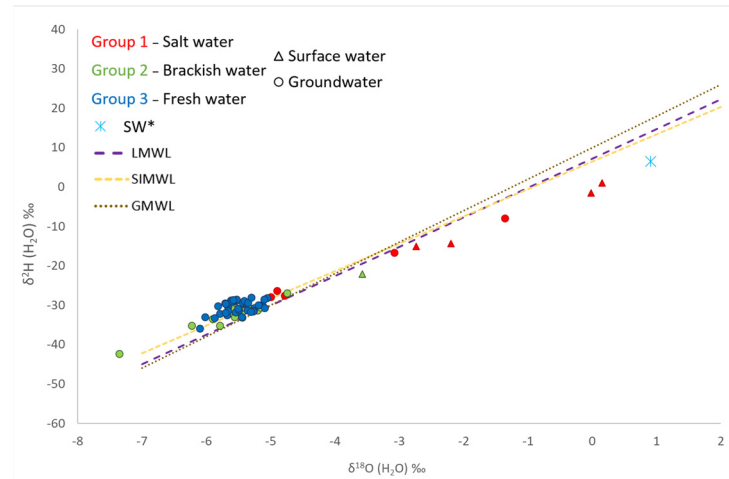


Figure 9. $\delta^2\text{H}\text{H}_2\text{O}$ vs. $\delta^{18}\text{O}\text{H}_2\text{O}$.

The predominantly meteoric origin of the water, as well as the salinization processes due to seawater intrusion, were confirmed by the isotopic results of sulfate (Figure 10a) and boron (Figure 10b). The following two main groupings were observed: one aligned with a meteoric-type sulfate origin, and a second group appeared to align toward the seawater isotopic signature, consistent with seawater intrusion processes [44].

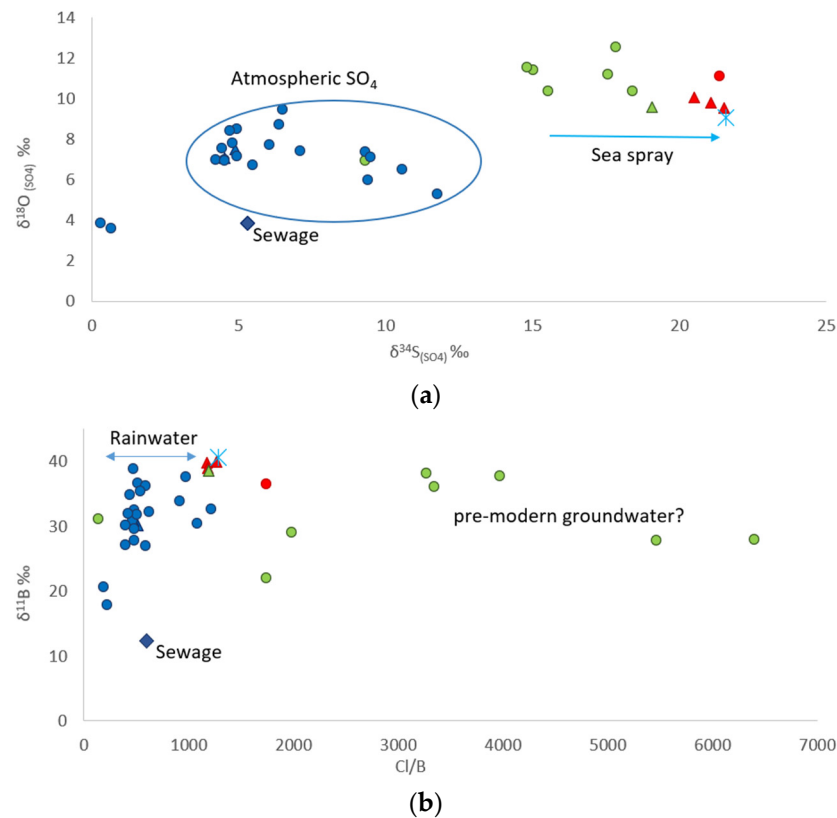


Figure 10. (a): $\delta^{18}\text{O}_{\text{SO}_4}$ vs. $\delta^{34}\text{S}_{\text{SO}_4}$, (b): $\delta^{11}\text{B}$ vs. Cl/B. Legend is presented in Figure 9.

Table 3. Results of isotope analyses; USD—urban sewage treatment plant discharges; gw—groundwater, sw—surface water.

ID	Type	Group	Date	$\delta^{11}\text{B}$ (‰)	$^{87}\text{Sr}/^{86}\text{Sr}$	$\delta^{34}\text{S}_{\text{SO}_4}$ (‰)	$\delta^{18}\text{O}_{\text{SO}_4}$ (‰)	$\delta^2\text{H}_{\text{H}_2\text{O}}$ (‰)	$\delta^{18}\text{O}_{\text{H}_2\text{O}}$ (‰)
1	usd	-	22 October 2020	12.30	0.71277	5.31	3.85	−30.9	−5.50
2	gw	3	15 October 2020	-	-	-	-	−29.0	−5.60
3	gw	3	16 October 2020	-	-	-	-	−28.6	−5.53
4	gw	3	2 October 2020	36.29	0.71350	4.80	7.82	−31.8	−5.55
4	gw	3	8 June 2022	-	-	-	-	−33.2	−5.88
6	gw	3	30 September 2020	32.61	0.71297	9.32	7.38	−30.8	−5.26
7d	gw	1	8 June 2022	-	-	-	-	−16.7	−3.08
7s	gw	2	29 September 2020	38.19	0.71129	17.58	11.20	−27.0	−4.74
7s	gw	2	8 June 2022	-	-	-	-	−42.3	−7.35
8d	gw	2	9 June 2022	-	-	-	-	−33.5	−5.90
8s	gw	2	29 September 2020	31.14	0.70963	-	-	−35.2	−5.79
8s	gw	2	9 June 2022	-	-	-	-	−35.2	−6.23
9d	gw	1	9 June 2022	-	-	-	-	−26.4	−4.90
9s	gw	1	29 September 2020	36.50	0.71017	21.36	11.12	−27.6	−4.79
9s	gw	1	9 June 2022	-	-	-	-	−27.9	−5.00
10	gw	3	30 September 2020	35.34	0.71486	9.41	5.98	−29.6	−5.70
11	gw	3	30 September 2020	27.05	0.71318	4.21	6.99	−29.4	−5.44
12	gw	3	29 September 2020	33.83	0.71305	7.09	7.43	−31.4	−5.26
13	gw	3	30 September 2020	37.54	0.71234	6.06	7.71	−33.0	−5.45
13	gw	3	8 June 2022	-	-	-	-	−32.5	−5.68
15	gw	3	30 September 2020	31.80	0.71287	4.94	7.16	−31.6	−5.31
16	gw	3	20 October 2020	31.98	0.71498	10.56	6.52	−28.7	−5.59
16	gw	3	8 June 2022	-	-	-	-	−30.2	−5.83
18	gw	3	2 October 2020	30.85	0.71329	4.52	6.98	−28.8	−5.53
19	gw	3	9 October 2020	26.90	0.71190	9.48	7.10	−29.5	−5.38
20	gw	3	9 October 2020	36.68	0.71105	11.76	5.27	−32.2	−5.79
21	gw	3	13 October 2020	-	-	-	-	−31.4	−5.67
22	gw	3	16 October 2020	-	-	-	-	−33.0	−6.02
23	gw	3	2 October 2020	38.81	0.71395	0.30	3.85	−28.1	−5.30
24	gw	3	1 October 2020	17.90	0.71270	6.38	8.73	−29.8	−5.41
24	gw	3	9 June 2022	-	-	-	-	−29.4	−5.43
26d	gw	2	9 June 2022	-	-	-	-	−31.7	−5.51
26s	gw	2	1 October 2020	27.84	0.71102	15.54	10.36	−31.3	−5.21
26s	gw	2	9 June 2022	-	-	-	-	−30.5	−5.16
27	gw	3	1 October 2020	20.62	0.71021	-	-	−36.0	−6.11

Table 3. Cont.

ID	Type	Group	Date	$\delta^{11}\text{B}$ (‰)	$^{87}\text{Sr}/^{86}\text{Sr}$	$\delta^{34}\text{S}_{\text{SO}_4}$ (‰)	$\delta^{18}\text{O}_{\text{SO}_4}$ (‰)	$\delta^2\text{H}_{\text{H}_2\text{O}}$ (‰)	$\delta^{18}\text{O}_{\text{H}_2\text{O}}$ (‰)
27	gw	3	10 June 2022	-	-	-	-	-35.3	-6.15
29	gw	2	9 October 2020	36.07	0.71197	14.83	11.54	-32.3	-5.66
30	gw	2	9 October 2020	22.06	0.71072	18.41	10.37	-30.8	-5.55
30	gw	2	10 June 2022	-	-	-	-	-31.0	-5.60
32	gw	2	13 October 2020	37.71	0.71172	15.03	11.40	-31.0	-5.48
33	gw	3	13 October 2020	-	-	-	-	-29.5	-5.71
34	gw	3	13 October 2020	-	-	-	-	-29.3	-5.35
35	gw	2	13 October 2020	-	-	-	-	-31.5	-5.42
36d	gw	1	10 June 2022	-	-	-	-	-8.0	-1.36
36s	gw	2	13 October 2020	27.96	0.71109	17.84	12.55	-30.8	-5.36
36s	gw	2	10 June 2022	-	-	-	-	-30.1	-5.37
37	gw	3	14 October 2020	30.48	0.71272	6.50	9.46	-30.5	-5.66
38	gw	3	14 October 2020	-	-	-	-	-31.35	-5.36
39	gw	3	14 October 2020	-	-	-	-	-30.7	-5.09
40	gw	3	14 October 2020	29.62	0.71261	4.94	8.49	-31.6	-5.27
40	gw	3	10 June 2022	-	-	-	-	-31.2	-5.50
42	gw	2	14 October 2020	-	-	-	-	-33.1	-5.56
43	gw	2	15 October 2020	-	-	-	-	-33.1	-5.45
44	gw	3	22 October 2020	34.90	0.71392	0.65	3.62	-28.8	-5.57
44	gw	3	15 October 2020	-	-	-	-	-28.7	-5.62
44	gw	3	8 June 2022	-	-	-	-	-29.7	-5.68
47	gw	3	15 October 2020	-	-	-	-	-28.9	-5.42
48	gw	3	16 October 2020	32.19	0.71211	4.52	6.96	-29.9	-5.20
49	gw	2	16 October 2020	29.02	0.71242	9.31	6.94	-30.5	-5.40
50	gw	3	20 October 2020	27.73	0.71202	4.43	7.54	-28.2	-5.06
51	gw	3	20 October 2020	30.19	0.71386	5.47	6.71	-32.0	-5.71
52	gw	3	22 October 2020	32.54	0.71209	4.68	8.41	-28.5	-5.10
53	gw	2	10 June 2022	-	-	-	-	-30.3	-5.15
54	gw	3	9 June 2022	-	-	-	-	-30.9	-5.51
55	sw	1	7 October 2020	38.94	0.70966	20.51	10.08	-14.3	-2.20
56	sw	3	7 October 2020	30.16	0.71278	4.88	7.52	-29.9	-5.16
57	sw	1	7 October 2020	39.88	0.70928	21.07	9.80	-15.1	-2.74
58	sw	1	7 October 2020	40.00	0.70920	21.53	9.57	1.0	0.15
59	sw	1	2 October 2020	-	-	-	-	-1.6	-0.02
60	sw	3	7 October 2020	30.88	0.71302	4.51	7.08	-29.7	-5.10
61	sw	2	7 October 2020	38.63	0.70999	19.06	9.60	-22.1	-3.58
SW*	sw	Lagoon	9 October 2020	40.65	0.70918	21.59	9.09	6.5	0.91

The $\delta^{11}\text{B}$ ranges from 12.30‰ in the water sample from the sewage treatment plant (Figure 10b) to 40.65‰ in sample SW*. The isotopic composition of boron confirms what has been described so far in Figure 10b. Some samples have higher Cl/B ratios than seawater with $\delta^{11}\text{B}$ near 40‰. In this case, salinization could result from mixing with less young groundwater that has evaporated and evolved, leading to higher Cl/B ratios [45].

Moreover, according to the $\delta^{11}\text{B}$ and $\delta^{18}\text{OSO}_4$ and $\delta^{34}\text{SSO}_4$, a possible significant recharge from the sewage treatment plant to the alluvial aquifer was ruled out.

The $^{87}\text{Sr}/^{86}\text{Sr}$ values exhibit a clear spatial variation (Figure 11a), showing a decreasing trend from the inner part of the plain towards the sea. This trend can be interpreted as the mixing of waters from different watersheds feeding the plain, providing a valuable recharge contribution compared to the zenithal one. This interpretation is supported by the linear correlation between $^{87}\text{Sr}/^{86}\text{Sr}$ values and the inverse of the Sr concentration (Figure 11b), indicating the progressive input of groundwater recharge from areas draining the San Vito Sandstone formation (namely Uri area), which has higher $^{87}\text{Sr}/^{86}\text{Sr}$ values (sample n. 16) overlapping with inputs derived from the Flumendosa watershed (sample n. 48), where carbonate formations are more extensive. The weak dispersion of the samples around the regression line suggests that contributions to recharge could come from multiple end members: Uri-type, seawater-type, and Flumendosa-type. This evidence is consistent with a previous study [46] conducted on surface waters in the area, which identified the Flumini Uri as the primary contributor to Flumendosa with an indicative contribution of 10% by weight for the tributary [46].

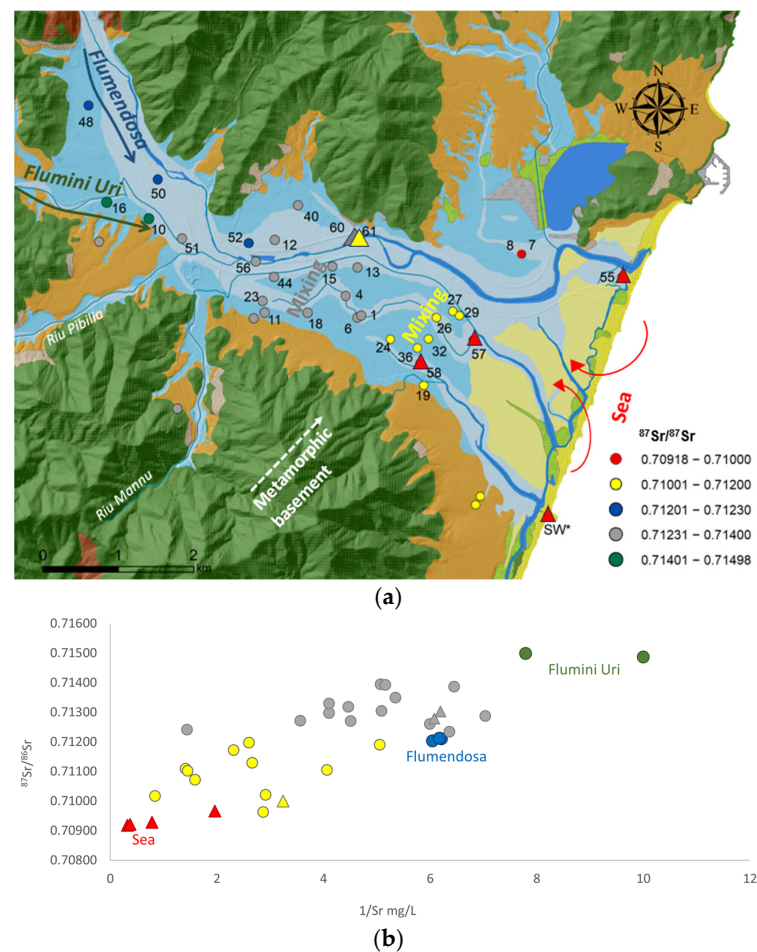


Figure 11. Interpretation of strontium isotopic values. Three different principal end members of the identified flow paths can be observed (for geological legend, refer to Figure 1). (a) spatialization of isotopic values classified according to the recognized pathways. (b) correlation between $^{87}\text{Sr}/^{86}\text{Sr}$ vs. $1/\text{Sr}$ indicating mixing processes among end-members.

As we moved the downgradient towards the coastal area, $^{87}\text{Sr}/^{86}\text{Sr}$ values tended to decrease, suggesting the significant contribution of seawater due to seawater intrusion. In fact, waters with the lowest isotopic values, below 0.71000, were predominantly found near the coast and could be attributed to strontium of seawater origin (in red in Figure 11).

An attempt to quantify recharge contributions from the above-identified end members (samples 16, 48, and SW*) was made by applying the Bayesian mixing model implemented in the SIAR (Stable Isotope Analysis in R) package [47,48] using the free language for statistical computing “R” [49]. The isotopic composition relative to $^{87}\text{Sr}/^{86}\text{Sr}$; $\delta^{11}\text{B}$, $\delta^{34}\text{S}_{\text{SO}_4}$ in the identified end members were included simultaneously in the mixing model. The Bayesian statistical models calculated confidence intervals for source apportionment while taking into account the uncertainty arising from the input [50–53]. This statistical model allows for the joint evaluation of multiple isotopes to define the recharge source contributions for each analyzed sample on a probabilistic basis, thereby reducing uncertainties. The simulation results are shown in Figure 12, outlining how water from different sources contributes to the groundwater system in the study area, with variations in composition and characteristics along its flow path through the aquifer.

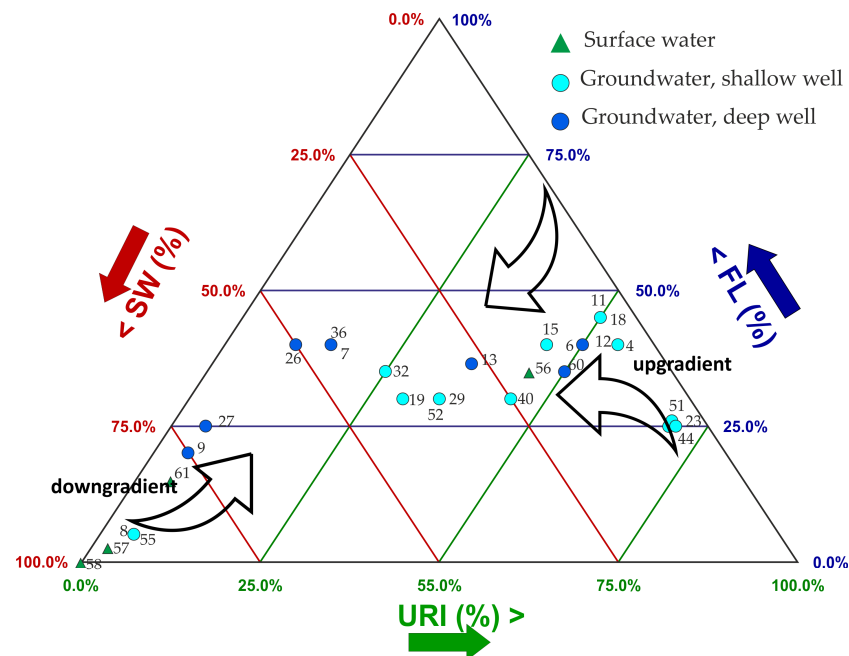


Figure 12. Contribution of different end members, URI (Uri-type), FL (Flumendosa-type), and SW (seawater-type), according to the Bayesian mixing model SIAR simulation.

The simulations indicate that, as water moves from the upgradient in the recharge area at the mouth of the Flumini Uri in the plain through the aquifer towards Muravera village, it tends to pick up components characteristic of the Flumendosa River. Near the Foxi area, the two components gradually decrease in favor of the seawater component. In this area of the plain, the Flumendosa River discharges into groundwater. However, downstream of sample 61, the river waters become saline, especially in the summer season, when there is limited runoff from upstream sources. This increased salinity contributes to the overall marine component in the groundwater, as the saline river water mixes with the groundwater in the final stretch of its course.

4. Conclusions

In this paper, the coastal area of Muravera in southeastern Sardinia was chosen as a pilot site for the application of a multidisciplinary investigative methodology aimed at identifying and quantifying the factors influencing seawater intrusion in the plain. After establishing that the zenithal recharge alone is insufficient to meet all withdrawals in the

plain, our methodology primarily focused on assessing lateral recharges from adjacent aquifers, with direct recharges from rivers crossing the plain and additional recharges from an urban wastewater treatment plant discharging into a channel.

The applied approach involved monthly monitoring campaigns to define piezometric trends and identify variations in chemical and physical parameters throughout an entire year. This information, combined with knowledge of the geometrical relationship between aquifers in the plain, allowed us to design water sampling for chemical and multi-isotopic analysis.

Monitoring data and geochemical results revealed a seawater edge extending about approximately 4 km inland from the coastline. Most water samples exhibited a sodium chloride composition, and the cation exchange processes recognized in samples near the Foxi or along the coastline confirmed the occurrence of seawater–freshwater mixing. There were no substantial differences in the geochemistry of waters from different aquifers, and the main variable parameter was chloride, which varied according to the distance from the coastline.

The results of $\delta^{18}\text{OH}_2\text{O}$ and $\delta^2\text{HH}_2\text{O}$, $\delta^{11}\text{B}$, and $\delta^{34}\text{SSO}_4$ indicated that meteoric water is the primary source of recharge and corroborate seawater–freshwater mixing processes. Strontium isotopic results provide valuable insights into the main flow path to the plain, which is further supported by piezometric trends, including the contribution from Flumendosa and Flumini Uri discharges into groundwater and seawater intrusion. The potential lateral contribution from the metamorphic basement and the Pleistocene alluvial aquifer were not excluded. Boron and sulfate isotopes ruled out sewage treatment plant discharge as a source of recharge to the alluvial aquifer.

The analysis of the boron isotope, B/Cl ratio, and binary graphs (especially SiO_2 vs. Sr and Na vs. Ca) suggest that certain brackish waters in the alluvial aquifer undergo very long water–rock interaction times, indicative of highly evolved groundwater. This could be interpreted with mixing processes with pre-modern seawater.

This comprehensive approach significantly enhances understanding of the studied system by identifying primary flow paths and recharge sources, which are crucial for informed decision-making regarding artificial recharge, a reduction in withdrawals, or stream management. Groundwater, particularly saline groundwater with an extended water–rock interaction time, may indicate slow recharge rates or a premodern seawater component, which is essential for addressing seawater intrusion.

Furthermore, these findings could also facilitate the calibration of a coupled numerical groundwater flow and solute transport model, which is essential for groundwater management in the context of climate change.

Overall, these results underscore the effectiveness of a holistic hydrogeological, geochemical, and isotopic approach to gain a better understanding of how to manage water effectively for safe and sustainable use. Given the important contribution made by the application of this approach, it can be easily replicated in other areas with similar contexts and problems.

Supplementary Materials: The following supporting information can be downloaded at: <https://www.mdpi.com/article/10.3390/w16081106/s1>, Table S1: Physical–chemical parameters and concentration of major and selected minor components dissolved in groundwater and surface water.

Author Contributions: Conceptualization, S.D.P., R.C., M.C.P. and C.A.; Methodology, S.D.P.; M.C.P., R.C., C.A., R.B., R.W., F.L. and F.P.; Validation, S.D.P., C.A., M.C.P. and R.B.; Formal Analysis, R.B.; Investigation, S.D.P., M.C.P., C.A., R.B., F.L. and F.P.; Resources, S.D.P., R.C., R.B. and F.P.; Data Curation, S.D.P., M.C.P., C.A. and R.B.; Writing—Original Draft Preparation, M.C.P., S.D.P. and C.A.; Writing—Review and Editing, S.D.P., M.C.P., R.C., C.A., R.B., R.W., F.L. and F.P.; Visualization, S.D.P., M.C.P., C.A. and R.B.; Supervision, S.D.P., C.A. and R.C.; Project Administration, S.D.P.; Funding Acquisition, S.D.P. and R.C. All authors have read and agreed to the published version of the manuscript.

Funding: Authors acknowledge the partial financial support under the National Recovery and Resilience Plan (NRRP), Mission 4 Component 2 Investment 1.5—Call for tender No. 3277 published on 30 December 2021 by the Italian Ministry of University and Research (MUR) funded by the European Union—NextGenerationEU. Project Code ECS0000038—Project Title eINS Ecosystem of Innovation for Next Generation Sardinia—CUP F53C22000430001—Grant Assignment Decree No. 1056 adopted on 23 June 2022 by the Italian Ministry of University and Research (MUR), and the partial financial support under the Agreement POA FSC 2014–2020—16.12.2019 among the ex MATTM—DGSTA and River Basin Authority (AdB) of Sardinia—Service for the protection and management of water resources, water services, and drought management—Regional Agency of the River basin district of Sardinia, Action 2.3.1 “Interventions to improve the quality of water bodies”, CUP F72G16000000001. The authors also acknowledge the Fulbright Specialist program (Project ID: FSP-P008493) for partially funding the Richard Wanty trip to Sardinia.

Data Availability Statement: The raw data supporting the conclusions of this article will be made available by the authors on request.

Acknowledgments: The authors acknowledge Mario Lorrari, Maurizio Testa, and Paolo Botti for their continuous support and their constructive suggestions. The authors thank Fabrizio Piscedda for his help during field activities and all the Muravera population for providing information and opening their homes to allow authors to conduct in situ measurements and sampling.

Conflicts of Interest: The authors declare no conflicts of interest.

References

1. Cao, T.; Han, D.; Song, X. Past, Present, and Future of Global Seawater Intrusion Research: A Bibliometric Analysis. *J. Hydrol.* **2021**, *603*, 126844. [[CrossRef](#)]
2. Post, V.E.A. Fresh and Saline Groundwater Interaction in Coastal Aquifers: Is Our Technology Ready for the Problems Ahead? *Hydrogeol. J.* **2005**, *13*, 120–123. [[CrossRef](#)]
3. Barlow, P.M.; Reichard, E.G. Saltwater Intrusion in Coastal Regions of North America. *Hydrogeol. J.* **2010**, *18*, 247–260. [[CrossRef](#)]
4. Mastrocicco, M.; Busico, G.; Colombani, N.; Vigliotti, M.; Ruberti, D. Modelling Actual and Future Seawater Intrusion in the Variconi Coastal Wetland (Italy) Due to Climate and Landscape Changes. *Water* **2019**, *11*, 1502. [[CrossRef](#)]
5. INEA. *Valutazione del Rischio di Salinizzazione dei Suoli e di Intrusione Marina Nelle Aree Costiere delle Regioni Meridionali in Relazione agli usi Irrigui*; Napoli, R., Vanino, S., Eds.; INEA Istituto Nazionale di Economia Agraria: Rome, Italy, 2011.
6. Perra, E.; Viola, F.; Deidda, R.; Caracciolo, D.; Paniconi, C.; Langousis, A. Hydrologic Impacts of Surface Elevation and Spatial Resolution in Statistical Correction Approaches: Case Study of Flumendosa Basin, Italy. *J. Hydrol. Eng.* **2020**, *25*, 05020032. [[CrossRef](#)]
7. Marras, P.A.; Lima, D.C.A.; Soares, P.M.M.; Cardoso, R.M.; Medas, D.; Dore, E.; De Giudici, G. Future Precipitation in a Mediterranean Island and Streamflow Changes for a Small Basin Using EURO-CORDEX Regional Climate Simulations and the SWAT Model. *J. Hydrol.* **2021**, *603*, 127025. [[CrossRef](#)]
8. Vengosh, A.; Kloppmann, W.; Marei, A.; Livshitz, Y.; Gutierrez, A.; Banna, M.; Guerrot, C.; Pankratov, I.; Raanan, H. Sources of Salinity and Boron in the Gaza Strip: Natural Contaminant Flow in the Southern Mediterranean Coastal Aquifer. *Water Resour. Res.* **2005**, *41*, 2004WR003344. [[CrossRef](#)]
9. Caschetto, M.; Colombani, N.; Mastrocicco, M.; Petitta, M.; Aravena, R. Nitrogen and Sulphur Cycling in the Saline Coastal Aquifer of Ferrara, Italy. A Multi-Isotope Approach. *Appl. Geochem.* **2017**, *76*, 88–98. [[CrossRef](#)]
10. Pennisi, M.; Bianchini, G.; Muti, A.; Kloppmann, W.; Gonfiantini, R. Behaviour of Boron and Strontium Isotopes in Groundwater–Aquifer Interactions in the Cornia Plain (Tuscany, Italy). *Appl. Geochem.* **2006**, *21*, 1169–1183. [[CrossRef](#)]
11. Yamanaka, M.; Kumagai, Y. Sulfur Isotope Constraint on the Provenance of Salinity in a Confined Aquifer System of the Southwestern Nobi Plain, Central Japan. *J. Hydrol.* **2006**, *325*, 35–55. [[CrossRef](#)]
12. Cary, L. Origins and Processes of Groundwater Salinization in the Urban Coastal Aquifers of Recife (Pernambuco, Brazil): A Multi-Isotope Approach. *Sci. Total Environ.* **2015**, *530–531*, 411–429. [[CrossRef](#)] [[PubMed](#)]
13. Bouchaou, L.; Michelot, J.L.; Vengosh, A.; Hsissou, Y.; Qurtobi, M.; Gaye, C.B.; Bullen, T.D.; Zuppi, G.M. Application of Multiple Isotopic and Geochemical Tracers for Investigation of Recharge, Salinization, and Residence Time of Water in the Souss–Massa Aquifer, Southwest of Morocco. *J. Hydrol.* **2008**, *352*, 267–287. [[CrossRef](#)]
14. Werner, A.D.; Bakker, M.; Post, V.E.A.; Vandenbohede, A.; Lu, C.; Ataie-Ashtiani, B.; Simmons, C.T.; Barry, D.A. Seawater Intrusion Processes, Investigation and Management: Recent Advances and Future Challenges. *Adv. Water Resour.* **2013**, *51*, 3–26. [[CrossRef](#)]
15. Jeon, S.-W.; Kang, J.; Jung, H.; Lee, J. Review of Seawater Intrusion in Western Coastal Regions of South Korea. *Water* **2021**, *13*, 761. [[CrossRef](#)]
16. Lim, J.-W.; Lee, E.; Moon, H.S.; Lee, K.-K. Integrated Investigation of Seawater Intrusion around Oil Storage Caverns in a Coastal Fractured Aquifer Using Hydrogeochemical and Isotopic Data. *J. Hydrol.* **2013**, *486*, 202–210. [[CrossRef](#)]

17. Castrignanò, A.; Buttafuoco, G.; Puddu, R. Multi-Scale Assessment of the Risk of Soil Salinization in an Area of South-Eastern Sardinia (Italy). *Precis. Agric.* **2008**, *9*, 17–31. [[CrossRef](#)]
18. Aru, A. *Nota illustrativa alla carta pedologica della Bassa Valle del Flumendosa con particolare riferimento ai suoli salsi di Muravera e Villaputzu (Cagliari)*; Centro Regionale Agrario Sperimentale: Cagliari, Italy, 1970; p. 41. Available online: https://www.igmi.org/carte-antiche/generali_italia/++theme++igm/immagini_antiche/biblioteca/B0004679.jpg (accessed on 13 March 2024).
19. Barbieri, G.; Barrocu, G.; Poledrini, C.; Uras, G. Salt Intrusion Phenomena in the South-East Coast of Sardinia. In *Geologia Applicata e Idrogeologia. Proceedings of the 8th Salt Water Intrusion Meeting*; Cotecchia V.: Bari, Italy, 1983; Volume 18, Parte II; pp. 315–323.
20. Barbieri, G. Hydrogeological and Geophysical Investigation for the Evaluation of Salt Intrusion Phenomena in Sardinia. 9th Salw Intr Meet Delfi. 1986, pp. 659–670. Available online: http://www.swim-site.nl/pdf/swim09/swim09_Barbieri_etal.pdf (accessed on 13 March 2024).
21. Careddu, M.B. Studio Della Contaminazione Di Acquiferi Costieri, Mediante Metodi Geofisici—Applicazione Alla Piana Di Muravera (Sardegna SE). Master’s Thesis, Università degli Studi di Cagliari, Cagliari, Italy, 1985.
22. Pilia, I. Studio idrogeologico della piana del Flumendosa (Sarrabus orientale). Master’s Thesis, Università degli Studi di Cagliari, Cagliari, Italy, 2002.
23. Deidda, G.P.; Ranieri, G.; Uras, G.; Cosentino, P.; Martorana, R. Geophysical Investigations in the Flumendosa River Delta, Sardinia (Italy)—Seismic Reflection Imaging. *Geophysics* **2006**, *71*, B121–B128. [[CrossRef](#)]
24. Balia, R.; Viezzoli, A. Integrated Interpretation If IP and TEM Data for Salinity Monitoring of Aquifers and Soil in the Coastal Area of Muravera (Sardinia, Italy). *Boll. Geofis. Teor. Appl.* **2015**, *56*, 31–42. [[CrossRef](#)]
25. Ardaù, F. Studio dei Fenomeni di Salinazione delle Acque Sotterranee Nella Piana di Muravera (Sardegna Sud-Orientale). Doctoral Thesis, Università degli Studi di Cagliari, Cagliari, Italy, 1995.
26. Ardaù, F.; Barbieri, G. Aquifer Configuration and Possible Causes of Salination in the Muravera Plain (SE Sardinia, Italy). Proceedings of 16th Salt Water Intrusion Meeting, Miedzyszdroje-Wo lin Island, Poland, 12–15 June 2000; pp. 11–18.
27. Ardaù, F.; Gavaudò, E. Recent Developments in Hydrogeological and Geophysical Research in the Muravera Coastal Plain (SE Sardinia, Italy). In Proceedings of the 17th 456 Salt Water Intrusion Meeting, Delft, The Netherlands, 6–10 May 2002.
28. Da Pelo, S.; Ghiglieri, G.; Buttau, C.; Biddau, R.; Cuzzocrea, C.; Funedda, A.; Carletti, A.; Vacca, S.; Cidu, R. Coupling 3D Hydrogeological Modelling and Geochemical Mapping for an Innovative Approach to Support Management of Aquifers. *Ital. J. Eng. Geol. Environ.* **2017**, *1*, 39–49. [[CrossRef](#)]
29. Porru, M.C.; Da Pelo, S.; Westenbroek, S.; Vacca, A.; Loi, A.; Melis, M.T.; Pirellas, A.; Buttau, C.; Arras, C.; Vacca, S.; et al. A Methodological Approach for the Effective Infiltration Assessment in a Coastal Groundwater. *Ital. J. Eng. Geol. Environ.* **2021**, *1*, 183–193. [[CrossRef](#)]
30. Arras, C.; (Department of Chemical and Geological Sciences, University of Cagliari, Monserrato (CA), Italy); Buttau, C.; (Department of Chemical and Geological Sciences, University of Cagliari, Monserrato (CA), Italy); Loi, A.; (Department of Chemical and Geological Sciences, University of Cagliari, Monserrato (CA), Italy); Funedda, A.; (Department of Chemical and Geological Sciences, University of Cagliari, Monserrato (CA), Italy); Lotti, F.; (Symple S.r.l.—Kataclima Srl Società Benefit, Vetralla (VT), Italy); Lorrari, M.; (Autonomous Region of Sardinia, Water Resources Protection and Management Service, Supervision of Water Services and Drought Management, Cagliari, Italy); Testa, M.; (Regional Environmental Protection Agency of Sardinia, ARPA Sardegna, Cagliari, Italy); Botti, P.; (Autonomous Region of Sardinia, Water Resources Protection and Management Service, Supervision of Water Services and Drought Management, Cagliari, Italy); Ghiglieri, G.; (Department of Chemical and Geological Sciences, University of Cagliari, Monserrato (CA), Italy); Da Pelo, S.; (Department of Chemical and Geological Sciences, University of Cagliari, Monserrato (CA), Italy). *CIS 1111 Detritico Alluvionale Plio-Quaternario di Muravera: Approfondimenti Sito-Specifici di Carattere Geologico e Idrogeologico e Modellazione Numerica*; Report: Approfondimenti idrogeologici funzionali alla valutazione dello stato quantitativo dei corpi idrici sotterranei del Distretto Idrografico della Sardegna, nell’ambito dell’aggiornamento del Piano di Gestione del Distretto Idrografico della Sardegna; DSCG—ADIS_STGRI. Unpublished work. 2022. (In Italian)
31. Puls, R.W.; Barcelona, M.J. Low-Flow (Minimal Drawdown) Ground-Water Sampling Procedures. Available online: <https://www.epa.gov/remedytech/low-flow-minimal-drawdown-ground-water-sampling-procedures> (accessed on 26 March 2024).
32. Nordstrom, D.K. Thermochemical Redox Equilibria of ZoBell’s Solution. *Geochim. Cosmochim. Acta* **1977**, *41*, 1835–1841. [[CrossRef](#)]
33. Pittalis, D.; Carrey, R.; Da Pelo, S.; Carletti, A.; Biddau, R.; Cidu, R.; Celico, F.; Soler, A.; Ghiglieri, G. Hydrogeological and Multi-Isotopic Approach to Define Nitrate Pollution and Denitrification Processes in a Coastal Aquifer (Sardinia, Italy). *Hydrogeol. J.* **2018**, *26*, 2021–2040. [[CrossRef](#)]
34. McArthur, J.M.; Howarth, R.J.; Bailey, T.R. Strontium Isotope Stratigraphy: LOWESS Version 3: Best Fit to the Marine Sr-Isotope Curve for 0–509 Ma and Accompanying Look-up Table for Deriving Numerical Age. *J. Geol.* **2001**, *109*, 155–170. [[CrossRef](#)]
35. Coplen, T.B. Guidelines and Recommended Terms for Expression of Stable-Isotope-Ratio and Gas-Ratio Measurement Results. *Rapid Commun. Mass Spectrom.* **2011**, *25*, 2538–2560. [[CrossRef](#)] [[PubMed](#)]
36. Appelo, C.A.J.; Postma, D. *Geochemistry, Groundwater and Pollution*, 2nd ed.; CRC Press: London, UK, 2005. [[CrossRef](#)]
37. Petelet-Giraud, E.; Négrel, P.; Aunay, B.; Ladouche, B.; Bailly-Comte, V.; Guerrot, C.; Flehoc, C.; Pezard, P.; Lofi, J.; Dörfliger, N. Coastal Groundwater Salinization: Focus on the Vertical Variability in a Multi-Layered Aquifer through a Multi-Isotope Fingerprinting (Roussillon Basin, France). *Sci. Total Environ.* **2016**, *566–567*, 398–415. [[CrossRef](#)] [[PubMed](#)]
38. Habtemichael, Y.T.; Fuentes, H.R. Hydrogeochemical Analysis of Processes Through Modeling of Seawater Intrusion Impacts in Biscayne Aquifer Water Quality, USA. *Aquat. Geochem.* **2016**, *22*, 197–209. [[CrossRef](#)]

39. Cherchi, A.; Da Pelo, S.; Ibba, A.; Mana, D.; Buosi, C.; Floris, N. Benthic Foraminifera Response and Geochemical Characterization of the Coastal Environment Surrounding the Polluted Industrial Area of Portovesme (South-Western Sardinia, Italy). *Mar. Pollut. Bull.* **2009**, *59*, 281–296. [[CrossRef](#)] [[PubMed](#)]
40. Cidu, R.; Biagini, C.; Fanfani, L. Mine Closure at Monteponi (Italy): Effect of the Cessation of Dewatering on the Quality of Shallow Groundwater. *Appl. Geochem.* **2001**, *16*, 489–502. [[CrossRef](#)]
41. Re, V.; Sacchi, E.; Martin-Bordes, J.L.; Aureli, A.; El Hamouti, N.; Bouchnan, R.; Zuppi, G.M. Processes Affecting Groundwater Quality in Arid Zones: The Case of the Bou-Areg Coastal Aquifer (North Morocco). *Appl. Geochem.* **2013**, *34*, 181–198. [[CrossRef](#)]
42. Giustini, F.; Brilli, M.; Patera, A. Mapping Oxygen Stable Isotopes of Precipitation in Italy. *J. Hydrol. Reg. Stud.* **2016**, *8*, 162–181. [[CrossRef](#)]
43. Craig, H. Isotopic Variations in Meteoric Waters. *Science* **1961**, *133*, 1702–1703. [[CrossRef](#)]
44. Dogramaci, S.S.; Herczeg, A.L.; Schi, S.L.; Bone, Y. Controls on $d34S$ and $d18O$ of Dissolved Sulfate in Aquifers of the Murray Basin, Australia and Their Use as Indicators of Flow Processes. *Appl. Geochem.* **2001**, *16*, 475–488. [[CrossRef](#)]
45. Cary, L.; Casanova, J.; Gaaloul, N.; Guerrot, C. Combining Boron Isotopes and Carbamazepine to Trace Sewage in Salinized Groundwater: A Case Study in Cap Bon, Tunisia. *Appl. Geochem.* **2013**, *34*, 126–139. [[CrossRef](#)]
46. Cidu, R.; Caboi, R.; Biddau, R.; Petrini, R.; Slejko, F.; Flora, O.; Stenni, B.; Aiuppa, A.; Parello, F. Caratterizzazione Idrogeochimica ed Isotopica e Valutazione della Qualità delle Acque Superficiali e Sotterranee Campionate nel Foglio 549 Muravera. In *Geochemical Baseline of Italy*; Ottonello, G., Ed.; Pacini Editore: Pisa, Italy, 2007.
47. Parnell, A.C.; Inger, R.; Bearhop, S.; Jackson, A.L. Source Partitioning Using Stable Isotopes: Coping with Too Much Variation. *PLoS ONE* **2010**, *5*, e9672. [[CrossRef](#)] [[PubMed](#)]
48. Parnell, A.C.; Phillips, D.L.; Bearhop, S.; Semmens, B.X.; Ward, E.J.; Moore, J.W.; Jackson, A.L.; Grey, J.; Kelly, D.J.; Inger, R. Bayesian Stable Isotope Mixing Models. *Environmetrics* **2013**, *24*, 387–399. [[CrossRef](#)]
49. R Core Team. *R: A Language and Environment for Statistical Computing*; R Foundation for Statistical Computing: Vienna, Austria, 2013; Available online: <http://www.R-project.org/> (accessed on 13 March 2024).
50. Ju, Y.; Mahlknecht, J.; Lee, K.-K.; Kaown, D. Bayesian Approach for Simultaneous Recognition of Contaminant Sources in Groundwater and Surface-Water Resources. *Curr. Opin. Environ. Sci. Health* **2022**, *25*, 100321. [[CrossRef](#)]
51. Jung, H.; Kim, Y.S.; Yoo, J.; Park, B.; Lee, J. Seasonal Variations in Stable Nitrate Isotopes Combined with Stable Water Isotopes in a Wastewater Treatment Plant: Implications for Nitrogen Sources and Transformation. *J. Hydrol.* **2021**, *599*, 126488. [[CrossRef](#)]
52. Biddau, R.; Dore, E.; Da Pelo, S.; Lorrain, M.; Botti, P.; Testa, M.; Cidu, R. Geochemistry, Stable Isotopes and Statistic Tools to Estimate Threshold and Source of Nitrate in Groundwater (Sardinia, Italy). *Water Res.* **2023**, *232*, 119663. [[CrossRef](#)] [[PubMed](#)]
53. Torres-Martínez, J.A.; Mora, A.; Mahlknecht, J.; Daesslé, L.W.; Cervantes-Avilés, P.A.; Ledesma-Ruiz, R. Estimation of Nitrate Pollution Sources and Transformations in Groundwater of an Intensive Livestock-Agricultural Area (Comarca Lagunera), Combining Major Ions, Stable Isotopes and MixSIAR Model. *Environ. Pollut.* **2021**, *269*, 115445. [[CrossRef](#)]

Disclaimer/Publisher’s Note: The statements, opinions and data contained in all publications are solely those of the individual author(s) and contributor(s) and not of MDPI and/or the editor(s). MDPI and/or the editor(s) disclaim responsibility for any injury to people or property resulting from any ideas, methods, instructions or products referred to in the content.